

Novel Topological Motifs and Superconductivity in Li-Cs System

Hong-Mei Huang, Qiang Zhu, Vladislav A. Blatov, Artem R. Oganov, Xiaoting Wei, Peng Jiang,* and Yan-Ling Li*



Cite This: *Nano Lett.* 2023, 23, 5012–5018



Read Online

ACCESS |

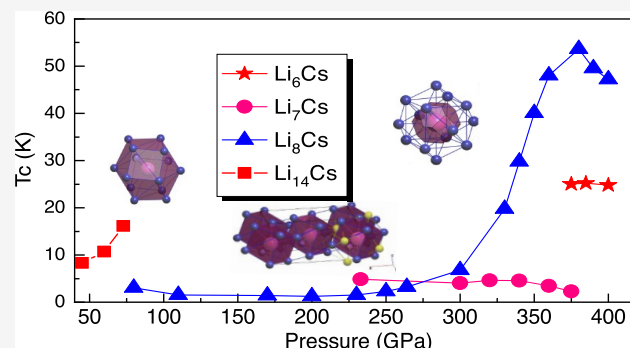
Metrics & More

Article Recommendations

Supporting Information

ABSTRACT: In this work, we determined the phase diagram and electronic properties of the Li-Cs system by using an evolutionary crystal structure prediction algorithm coupled with first-principles calculations. We found that Li-rich compounds are more easily formed in a wide range of pressures, while the only predicted Cs-rich compound LiCs_3 is thermodynamically stable at pressures above 359 GPa. A topological analysis of crystal structures concludes that both Li_6Cs and Li_{14}Cs have a unique topology that has not been reported in existing intermetallics. Of particular interest is the fact that four Li-rich compounds (Li_{14}Cs , Li_8Cs , Li_7Cs , and Li_6Cs) are found to be superconductors with a high critical temperature (~ 54 K for Li_8Cs at 380 GPa), due to their peculiar structural topologies and notable charge transfer from Li to Cs atoms. Our results not only extend an in-depth understanding of the high-pressure behavior of intermetallic compounds but also provide a new route to design new superconductors.

KEYWORDS: superconductivity, topological motif, intermetallic compound, high pressure, charge transfer, first-principles calculations



Pressure, as a thermodynamic parameter, can not only be used to dramatically alter the atomic and electronic structure of materials, making a rich phase diagram and thus exhibiting exotic physical or chemical properties^{1–11} but also to design novel functional materials not accessible under normal conditions, enriching the realms of superconductivity,^{12–19} photovoltaic materials,^{20,21} superhardness,^{22–24} and high energy density.^{25,26} Alkali metals, long thought to be “simple”, display nontrivial behavior under pressure.²⁷ Of these metals, lithium, as the “simplest” metal under ambient conditions, undergoes a series of symmetry-breaking phase transitions under compression, exhibiting anomalous electronic properties, including s–p orbital mixing,²⁸ superconductivity,^{29,30} and highly counterintuitive metal-to-semiconductor transitions.^{6,31} Na enters a wide-gap insulating state above 180 GPa, becoming transparent to visible light.⁷ The high-pressure behavior of cesium has also been extensively studied.^{32,33} The complex structural and electronic behavior of cesium is closely related to pressure-driven electrons transfer from the 6s to the 5d band (referred to as a s–d transition).³³ The s–d transition strongly enhances the d character of cesium, enabling unusual chemical reactions with other elements; in particular, this makes cesium more electronegative than lithium and sodium at high pressure.³⁴ Is it then possible to generate a Li-Cs compound by means of external pressure since no Li-Cs compound exists under ambient conditions? There have been two theoretical studies based on density functional theory (DFT) attempting to explore ordered stoichiometric phases in

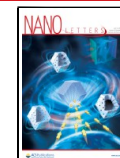
the Li-Cs system at high pressure using crystal structure prediction methods.^{35,36} Zhang and Zunger predicted that both Li_nCs and LiCs_n can be stabilized by a pressure-induced charge transfer from Cs to Li.³⁵ Another study proposed that stable intermetallic Li_nCs ($n = 1–5$) compounds can be formed above 100 GPa because pressure promotes a large charge transfer from Li to Cs, leading to anionic Cs with a formal charge beyond -1 .³⁶ A subsequent experiment claimed that at low pressure LiCs compound can be formed, where electrons are donated from Cs to Li, resulting in a rare formal oxidation state of -1 for Li.³⁷ Obviously, the charge transfer suggested in these studies remains controversial, which motivates us to perform a further theoretical study to obtain an accurate thermodynamic phase diagram and understand this discrepancy in charge transfer.

In order to determine the phase diagram, one needs to find the candidate structures, which are likely to be formed in the entire compositional space under investigation. Two approaches have been widely used for this purpose. One of them requires performing structure searches for many different

Received: March 7, 2023

Revised: May 16, 2023

Published: May 22, 2023



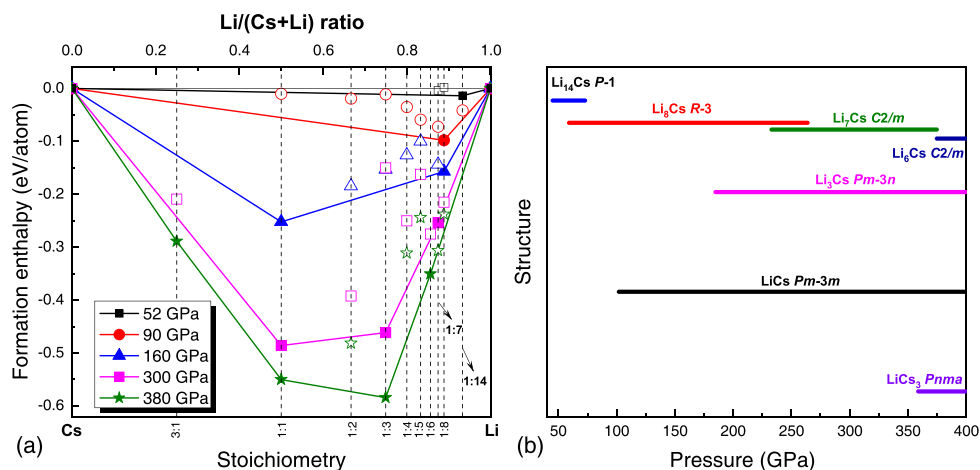


Figure 1. (a) Convex hull diagram for the Li-Cs system at selected pressures. At a given pressure, the compounds located on the convex hull are thermodynamically stable. (b) Pressure–composition phase diagram of the Li-Cs system.

compositions, requiring many separate calculations to adequately sample the composition space. In practice, only a limited set of compositions are considered in most calculations, as was done in both of the previous works on the Li-Cs system.^{35,36} On the other hand, a variable-composition search, in which both the compositions (which now is not just one global minimum but a set of compositions that are stable at different chemical potential ranges) and the corresponding structures are optimized, has been developed and successfully applied to many systems.^{8,19,21,38–41} Our studies showed that the second method is particularly efficient and reliable.

In this work, we constructed the thermodynamic phase diagram of the Li-Cs system in a wide range of pressures and zero temperature by using both variable-composition and fixed-composition searches with the USPEX code.^{38–40} Our results suggest that the stable intermetallic compounds in the Li-Cs system begin to appear at much lower pressure (~45 GPa) than in previous predictions.^{35,36} In addition to the previously predicted LiCs, Li₃Cs, and Li₇Cs compounds, three novel Li-rich compounds (Li₁₄Cs, Li₈Cs, and Li₆Cs) and the Cs-rich compound LiCs₃ were discovered for the first time. Besides, novel topological motifs in Li-rich compounds were revealed via topological analysis of crystal structures. Remarkably, an unexpectedly high critical temperature of 54 K was found in Li₈Cs under high pressure.

The stable Li-Cs compounds and their structures were explored by using the *ab initio* evolutionary algorithm USPEX,^{38–40} which can simultaneously find stable stoichiometries and the corresponding structures in multicomponent systems. More computational details of the crystal structure prediction and DFT calculations can be found in the Supporting Information (SI), which gives some necessary references.^{42–47} In these calculations, all stoichiometries were allowed (with the constraint that the total number of atoms in the primitive cell be below 32 atoms), and calculations were performed at 50, 80, 100, 150, 200, 250, 300, and 360 GPa. A pressure–composition phase diagram (convex hull) of the Li-Cs system is given in Figure 1a.

At normal conditions, no Li-Cs compounds are formed, because lithium and cesium have similar Pauling electronegativities, and because of their very different atomic radii, there is virtually no Li-Cs solid solubility, according to the Hume–Rothery rule.⁴⁸ Obviously, high pressure favors the

formation of Li-Cs compounds, which is attributed to pressure-induced changes of their atomic radii and electronegativities (discussed later). Using variable-composition evolutionary searches, we found that Li₁₄Cs, Li₈Cs, Li₇Cs, Li₆Cs, Li₃Cs, LiCs, and LiCs₃ become thermodynamically stable in different pressure ranges: Li₁₄Cs (45–73 GPa), Li₈Cs (59–264 GPa), Li₇Cs (233–375 GPa), Li₆Cs (>375 GPa), Li₃Cs (>185 GPa), LiCs (>102 GPa), and LiCs₃ (>359 GPa) (see Figure 1b). Therefore, the predicted convex hull diagrams suggest that Li-rich compounds are more easily formed in a wide range of pressures while the only Cs-rich compound LiCs₃ is thermodynamically stable under ultrahigh pressure. The reported Cmmm-Li₇Cs³⁵ is no longer thermodynamically stable due to the occurrence of two new compounds (Li₁₄Cs and Li₈Cs) on the convex hull under rather lower pressure. Unexpectedly, we found that no structural phase transition occurs in any of the stable Li-Cs compounds in pressure ranges of their stability. The crystal structure parameters of stable Li-Cs compounds are shown in Table S1 in the SI. LiCs adopts a well-known CsCl-type structure appearing in many ionic and intermetallic phases. The Li₃Cs has an A15-type structure (space group $Pm\bar{3}n$, two formula units per cell), which differs from Miao's result³⁶ since stability field of Li₃Cs is moved to much higher pressures due to the discovery of two new compounds at lower pressure here. LiCs₃ has a Pd₃Si-type structure (space group $Pnma$, four formula units per cell). We note that, however, there are no available prototypical compounds for Li₁₄Cs, Li₈Cs, Li₇Cs, and Li₆Cs. For all the newly predicted structures, the calculated phonon dispersion curves confirmed their dynamical stability (see Figures S1–S6 in the SI). All of the Li-rich compounds possess low-frequency phonon modes at high symmetry points in the Brillouin zone (BZ), which is favorable for strong electron–phonon (e–p) coupling in them. Surprisingly, our theoretical calculations show that Li₈Cs is dynamically stable up to 400 GPa and has a high superconducting critical temperature under such high compression (discussed later).

To identify the underlying topological features of crystal structures, we conducted a geometrical and topological analysis of the crystal structures of Li-Cs compounds using the ToposPro package.⁴⁹ More theoretical details are described in the SI, including relevant references.^{49–53} The sizes of both Li and Cs are much smaller in our compounds under

pressure than in pure alkali metals under normal conditions. For example, the size of Cs atoms in the Li environment estimated as the radius of Cs spherical domain (R_{sd} , i.e. radius of a sphere with the volume of an atomic Voronoi polyhedron) strongly decreases with pressure (see Figure S7 in the SI). In the cases of Li_8Cs , Li_7Cs , and LiCs , the topology of the whole framework corresponds to the 14-coordinated body-centered cubic lattice (referred as **bcu-x**) (Figure 2a). Importantly, all

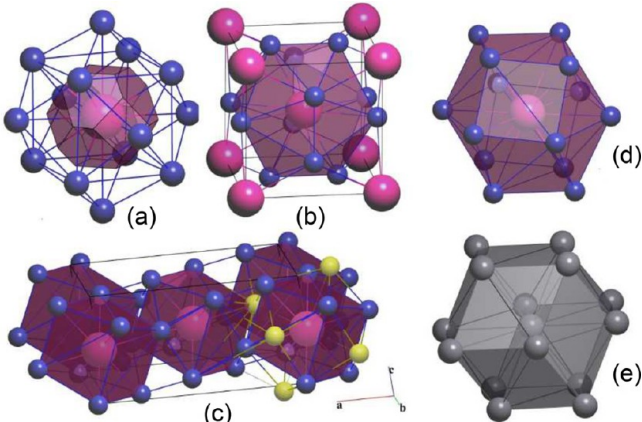


Figure 2. Topological motifs with environment of Cs atoms by Li atoms in (a) Li_8Cs , (b) Li_3Cs , (c) Li_6Cs , and (d) Li_{14}Cs . The Voronoi polyhedron (a) and coordination polyhedra (b–d) of Cs atoms are shown in red. (e) Coordination polyhedron of an atom in an undistorted **bcu-x** net. The yellow Li atoms (c) indicate additional contacts of the Cs atom, which complement its coordination to $8 + 6$.

pure alkali metals also have **bcu-x** topologies of the maximum cubic symmetry ($\text{Im}\bar{3}m$) at ambient pressure, while the Li_8Cs **bcu-x** motif is rhombohedrally distorted. The same applies to Li_7Cs , which has monoclinic ($\text{C}2/m$) symmetry but a rather regular **bcu-x** motif (Figure S8 in the SI). The maximum $\text{Im}\bar{3}m$ symmetry is realized only in LiCs . Mixed alkali intermetallics

tend to adopt Laves-phase motifs with even higher coordination numbers of the larger alkali atom (also Cs) of 15–16. In the compounds considered here, the coordination numbers of Li and Cs atoms vary in the ranges 9–14 and 12–14, respectively, so the high pressure obviously decreases too high coordination numbers >14 because the sizes of Li and Cs become closer. Other compounds have individual topologies.

The most common is the topological type of β -W (also known as the Cr_3Si structure type), which is adopted in Li_3Cs . This is the only structure where Cs has an icosahedral environment by Li atoms and the smallest coordination number of 12 (see Figure 2b). The topology of the Cs-rich LiCs_3 is characterized by a more special type of 9,13,13T2, which occurs in intermetallics with smaller atoms (like Pd_3Si) at ambient pressure. In this structure, Cs atoms have coordination number 13, but they are connected with 10 other Cs atoms and only 3 Li atoms. Li_6Cs has a unique topology, which does not occur in other intermetallics; however, the multilevel topological analysis shows that it contains a distorted body-centered (bcu) motif with coordination numbers of all atoms equal to 8 (cubic coordination) and some additional weaker contacts (see Figure 2c). This means that high pressure distorts the **bcu-x** motif and breaks weaker six contacts in its $8 + 6$ coordination but keeps the stronger eight contacts. Finally, the highest Li-rich composition, Li_{14}Cs , has a unique topology at all levels of interatomic interaction; it is hardly possible to find its relations to any other intermetallics. However, here Cs atoms also have a slightly distorted environment by Li atoms (see Figure 2d), which is typical for the **bcu-x** topology (see Figure 2e). Thus, body-centered motifs remain important for all Li-rich compounds predicted here. Note that new topologies are quite rare in the binary intermetallics. We have deposited this new topology to the TopCryst database system (<https://topcryst.com>)⁵⁴ under the name 12,13⁴,14³T1 according to the TopCryst nomenclature.

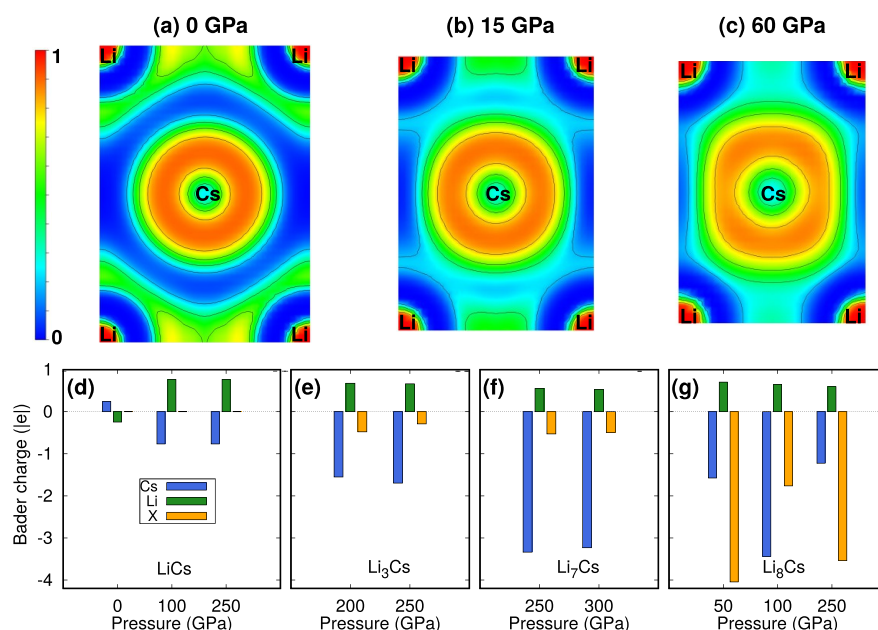


Figure 3. ELF maps of $\text{Pm}\bar{3}m$ LiCs at (a) 0 GPa, (b) 15 GPa, and (c) 60 GPa and Bader charge analysis on (d) $\text{Pm}\bar{3}m$ LiCs , (e) $\text{Pm}\bar{3}n$ Li_3Cs , (f) $\text{C}2/m$ Li_7Cs , and (g) $\text{R}\bar{3}$ Li_8Cs at various pressures. X denotes the total charge of the basins of non-nuclear charge density maxima.

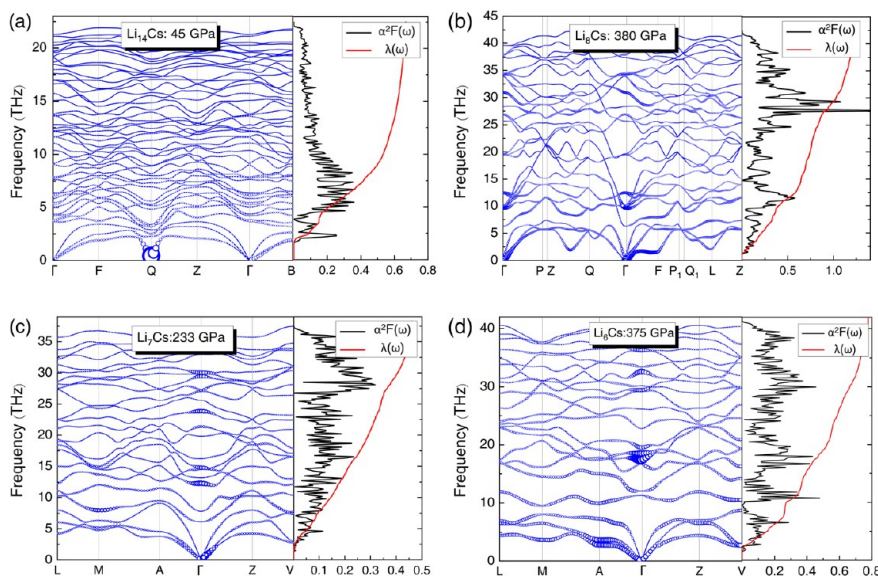


Figure 4. Phonon dispersions, electron–phonon coupling, Eliashberg spectral function $\alpha^2F(\omega)$, and cumulative frequency-dependent coupling $\lambda(\omega)$ for superconducting Li-rich compounds: (a) Li_{14}Cs at 45 GPa, (b) Li_8Cs at 380 GPa, (c) Li_7Cs at 233 GPa, and (d) Li_6Cs at 375 GPa. The area of the circles is proportional to the magnitude of electron–phonon couplings λ_{qv} .

In order to resolve the nature of chemical bonding in the Li–Cs compounds, we analyzed their electron localization functions (ELFs) and Bader charges under various conditions. We first considered the $Pm\bar{3}m$ LiCs under ambient conditions. Both ELF and charge density maps are consistent with metallic bonding. The general trend in the topology of ELF in elemental metals is location of its attractors in the tetrahedral or octahedral holes within the crystal structure,⁵⁵ which applies to $Pm\bar{3}m$ LiCs as well. The ELF map (Figure 3a) is composed of three localization attractors, namely the Li core, the Cs core, and the shared electrons in the $[\text{Cs}_4\text{Li}_2]$ octahedral interstitials. With increasing pressure, the shared electrons tend to be depleted, while the basin of the Cs core gradually expands and the Li core slightly shrinks (Figure 3b,c). This indicates that Cs gains more electrons upon compression. Accordingly, the Bader charge of Cs in $Pm\bar{3}m$ LiCs changes sign from +0.25 lel at 0 GPa to −0.77 lel at 250 GPa, as shown in Figure 3d. According to the recent work,³⁴ the electronegativity difference between Li and Cs changes from 1.41 eV at 0 GPa (Li is more electronegative) to 0.03 eV at 50 GPa and to −0.39 eV at 200 GPa (Cs is more electronegative), which indicates that under pressure there will be charge transfer from Li to Cs.

The same feature of charge transfer can also be observed in $Pnma$ LiCs_3 (see Figure S9 in the SI). Our results thus satisfactorily reconcile the controversies in recent works.^{35,36} As shown in ref 34, pressure greatly affects electronegativities of the elements and thus affects chemical bonding and the direction of charge transfer. Finally, we also analyzed the charge transfer for all stable compounds (Figure 3e–g). For the Li-rich compounds (e.g., Li_3Cs , Li_7Cs , and Li_8Cs), there exist non-nuclear maxima of electron density. For convenience, we call them X-basins in Figure 3e–g. It is evident that Cs tends to gain more electrons with the increasing concentration of Li in the system, which is similar to Miao’s results.³⁶ For instance, the Bader charge of Cs decreases from −0.77 lel for LiCs to −1.70 lel for Li_3Cs and to −3.34 lel for Li_7Cs at 250 GPa. However, the trend is not necessarily monotonic. For Li_8Cs , the Bader charge of Cs is −1.57 lel at 50 GPa, −3.44 lel

at 100 GPa, and −1.23 lel at 250 GPa. These features are very similar to what has been found in elemental Li.⁶

As shown in Figures S10–S14, electronic structure calculations suggest that all predicted compounds are metallic. From the projected density of states (PDOS) given in Figures S10–S13, one can see that these compounds have similar electronic structures. Dominant contributions to the DOS near the Fermi level come from the Cs d electrons, Li p electrons, and Li s electrons, whereas the Cs s and Cs p electrons make minor contributions, due to s→p transition in Li and s→d transition in Cs. Such charge transfer or charge rearrangement has been observed in the Al–O system under pressure.⁵⁶ The pressure-driven charge transfer makes new compounds favorable ones energetically. For Li_{14}Cs , a considerable feature is the appearance of a flat band lying just at the Fermi level around the Γ , Q , and Z points, especially along the Γ –F direction in BZ. As for Li_8Cs and Li_7Cs , flat and steep bands were observed around the Γ point near the Fermi level. The coexistence of flat and steep bands near the Fermi level is a favorable condition for enhancing Cooper pair formation and superconductivity. A remarkable feature of the electronic structure in the high- T_c phase is the appearance of small pockets of the Fermi level.

Observed low-frequency phonon modes, a nested Fermi surface, and steep and flat energy bands near the Fermi level stimulate our interest in the potential superconductivity of Li-rich compounds. All Li-rich compounds consist of three-periodic lithium frameworks with the interstitial cesium atoms, which are helpful for enhancing the e–p coupling when applying pressure, giving Li-rich compounds (except for Li_3Cs) superconductivity. Our calculations indicate that both LiCs and Li_3Cs are not superconductors in their pressure ranges of stability because of a low e–p coupling. Using the phonon line width γ_{qv} , we can identify the contribution to the e–p interaction parameter λ from each mode (λ_{qv}) based on the relation $\lambda_{qv} = \frac{\gamma_{qv}}{\pi N(0)\omega_{qv}^2}$. Here, $N(0)$ is the density of states at the Fermi surface. The calculated phonon dispersion, Eliashberg spectral function $\alpha^2F(\omega)$, integrated $\lambda(\omega)$, and λ_{qv}

of four compounds at a given pressure are plotted in Figure 4. The Eliashberg spectral function $\alpha^2F(\omega)$ is closely related to the λ_{qv} , resulting in the location of peaks of $\alpha^2F(\omega)$ matching the distribution of the λ_{qv} magnitudes. The high values of λ_{qv} lie at the high-symmetry point Γ for Li_8Cs , Li_7Cs , and Li_6Cs but point Q for Li_{14}Cs . From Figure 4, we conclude that the vibrational modes from Li atoms dominate the e-p coupling, which is similar to the hydrogen atoms in superconducting hydrogen-rich hydrides. Differing from $\text{P}\bar{\text{l}}\text{-Li}_{14}\text{Cs}$, the e-p coupling processes in $\text{R}\bar{3}\text{-Li}_8\text{Cs}$, $\text{C}2/m\text{-Li}_7\text{Cs}$, and $\text{C}2/m\text{-Li}_6\text{Cs}$ are distributed over a broad frequency range. In the case of Li_8Cs , the Eliashberg function has two main peaks at 380 GPa, a broad peak in the 22–33 THz region and a second peak in the 9–15 THz region. Their contributions to λ are 0.28 and 0.23, respectively, accounting for about 51% of the total λ , while acoustic modes contribute about 21.5% of the total λ . In brief, the e-p interaction is mainly due to strong coupling to the high-frequency optical modes, although the acoustic phonons also make a noticeable contribution: that is, the Li atoms dominate superconductivity, due to their prominent contributions to the e-p interaction. Phonons from the Li atoms together with the electrons from the Cs d and Li p states provide a strong electron–phonon coupling necessary for strong superconductivity in the Li-Cs system.

The superconducting transition temperature T_c was estimated using the Allen and Dynes formula,⁵⁷ namely, $T_c = \frac{\omega_{\log}}{1.2} \exp\left[-\frac{1.04(1+\lambda)}{\lambda - \mu^*(1+0.62\lambda)}\right]$, by virtue of the value of λ determined above and a typical value of 0.11 for μ^* (effective screened Coulomb repulsion constant) along with the calculated ω_{\log} . This formula has been successfully used to predict the T_c for various systems that have been subsequently proved experimentally.^{9,58,59} Applying pressure to the Li-Cs system clearly leads to λ and T_c changing remarkably. The calculated highest value of T_c is the considerable 54 K in Li_8Cs at 380 GPa (see Figure 5). High T_c is attributed to a peculiar structural feature. As mentioned above, the structures of superconducting Li-rich compounds reported here contain the three-periodic lithium frameworks with interstitial cesium atoms (CN up to 14), which is beneficial to enhance the e-p

coupling and thus T_c when applying pressure, providing a new idea for the design of new types of superconductors.

To sum up, the thermodynamic phase diagram and the electronic properties of the Li-Cs system were determined by using the evolutionary crystal structure prediction method coupled with first-principles total energy calculations. The Li-Cs system favors the formation of Li-rich compounds compared to the Cs-rich side in a wide window of pressures (only the predicted LiCs_3 compound is thermodynamically stable above 359 GPa). Seven thermodynamically stable compounds can be stabilized because of pressure-induced charge transfer. For Li-rich compounds, the body-centered motifs were uncovered via a topological analysis of crystal structures. Interestingly, both Li_{14}Cs and Li_6Cs possess unique topologies. Four Li-rich compounds, including Li_{14}Cs , Li_8Cs , Li_7Cs , and Li_6Cs , display superconductivity, which is attributed to the strong e-p coupling between electrons from Cs d, Li p, and Li s and phonons related mostly to vibrations of Li atoms. This study not only unravels the topological property of crystal structures and chemical bonding in the Li-Cs system under pressure but also demonstrates its unexpected superconductivity, which provides a new platform for exploring novel chemistry and physics in these fascinating intermetallic compounds.

■ ASSOCIATED CONTENT

SI Supporting Information

The Supporting Information is available free of charge at <https://pubs.acs.org/doi/10.1021/acs.nanolett.3c00875>.

Computational methods and details, phonon spectra, PHDOS, band structures, and PDOS of $\text{P}\bar{\text{l}}\text{-Li}_{14}\text{Cs}$, $\text{R}\bar{3}\text{-Li}_8\text{Cs}$, $\text{C}2/m\text{-Li}_7\text{Cs}$, and $\text{C}2/m\text{-Li}_6\text{Cs}$ at selected pressures, phonon spectra and band structures of $\text{Pm}3n\text{-Li}_3\text{Cs}$ and Pnma-LiCs_3 at selected pressures, pressure-dependent R_{sd} of Cs atoms, Voronoi polyhedron of the Cs atom surrounded by 14 Li atoms in Li_7Cs , pressure-dependent Bader charge of the Cs atom in Pnma-LiCs_3 , and crystal structures of stable Li-Cs compounds ([PDF](#))

■ AUTHOR INFORMATION

Corresponding Authors

Peng Jiang – School of Physics and Electronic Engineering, Jiangsu Normal University, Xuzhou 221116, People's Republic of China; orcid.org/0000-0002-4291-608X; Email: pjiang@jsnu.edu.cn

Yan-Ling Li – School of Physics and Electronic Engineering, Jiangsu Normal University, Xuzhou 221116, People's Republic of China; orcid.org/0000-0002-0144-5664; Email: ylli@jsnu.edu.cn

Authors

Hong-Mei Huang – School of Physics and Electronic Engineering, Jiangsu Normal University, Xuzhou 221116, People's Republic of China

Qiang Zhu – Department of Physics and Astronomy, University of Nevada Las Vegas, Las Vegas, Nevada 89154-4002, United States

Vladislav A. Blatov – Samara Center for Theoretical Materials Science (SCTMS), Samara State Technical University, Samara 443100, Russia; orcid.org/0000-0002-4048-7218

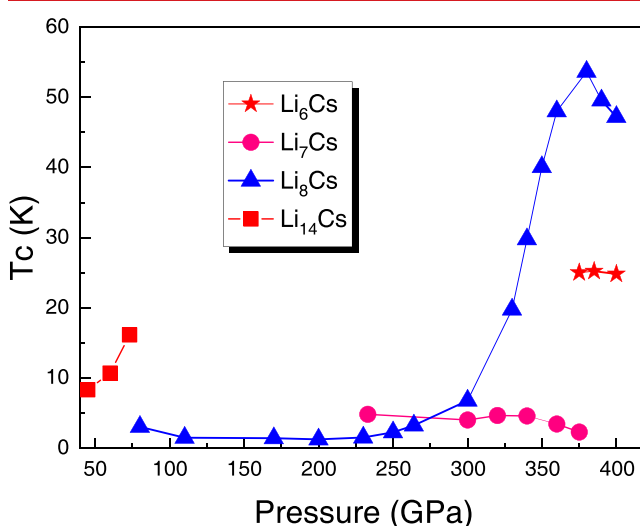


Figure 5. Superconducting critical temperature (T_c) of Li_{14}Cs , Li_8Cs , Li_7Cs , and Li_6Cs at high pressure. The T_c value of Li_8Cs reaches 54 K at 380 GPa.

Artem R. Oganov – Skolkovo Institute of Science and Technology, Moscow 121205, Russia; orcid.org/0000-0001-7082-9728

Xiaoting Wei – ICMD, Northwestern Polytechnical University, Xi'an 710072, People's Republic of China

Complete contact information is available at:
<https://pubs.acs.org/10.1021/acs.nanolett.3c00875>

Notes

The authors declare no competing financial interest.

ACKNOWLEDGMENTS

We acknowledge support from the National Natural Science Foundation of China (Grant Nos. 12074153, 11674131, and 12204202), the Natural Science Foundation of Jiangsu Province (Grant No. BK20220679), the and Natural Science Fund for Colleges and Universities in Jiangsu Province (Grant No. 22KJB140010). A.R.O. acknowledges funding from the Russian Science Foundation (grant 19-72-30043).

REFERENCES

- (1) Zhang, W.; Oganov, A. R.; Goncharov, A. F.; Zhu, Q.; Boulfelfel, S. E.; Lyakhov, A. O.; Stavrou, E.; Somayazulu, M.; Prakapenka, V. B.; Konôpková, Z. Unexpected stable stoichiometries of sodium chlorides. *Science* **2013**, *342*, 1502–1505.
- (2) Struzhkin, V. V.; Eremets, M. I.; Gan, W.; kwang Mao, H.; Hemley, R. J. Superconductivity in dense lithium. *Science* **2002**, *298*, 1213–1215.
- (3) Miao, M.-s. Caesium in high oxidation states and as a p-block element. *Nat. Chem.* **2013**, *5*, 846–852.
- (4) Eshet, H.; Khalilullin, R. Z.; Kühne, T. D.; Behler, J.; Parrinello, M. Microscopic origins of the anomalous melting behavior of sodium under high pressure. *Phys. Rev. Lett.* **2012**, *108*, 115701.
- (5) Pickard, C. J.; Needs, R. J. Predicted pressure-induced s-band ferromagnetism in alkali metals. *Phys. Rev. Lett.* **2011**, *107*, 087201.
- (6) Matsuoka, T.; Shimizu, K. Direct observation of a pressure-induced metal-to-semiconductor transition in lithium. *Nature* **2009**, *458*, 186–189.
- (7) Ma, Y.; Eremets, M.; Oganov, A. R.; Xie, Y.; Trojan, I.; Medvedev, S.; Lyakhov, A. O.; Valle, M.; Prakapenka, V. Transparent dense sodium. *Nature* **2009**, *458*, 182–185.
- (8) Dong, X.; Oganov, A. R.; Goncharov, A. F.; Stavrou, E.; Lobanov, S.; Saleh, G.; Qian, G.-R.; Zhu, Q.; Gatti, C.; Deringer, V. L.; et al. A stable compound of helium and sodium at high pressure. *Nat. Chem.* **2017**, *9*, 440–445.
- (9) Liu, X.; Jiang, P.; Wang, Y.; Li, M.; Li, N.; Zhang, Q.; Wang, Y.; Li, Y.-L.; Yang, W. T_c up to 23.6 K and robust superconductivity in the transition metal δ -Ti phase at megabar pressure. *Phys. Rev. B* **2022**, *105*, 224511.
- (10) Wang, X.; Wang, Y.; Wang, J.; Pan, S.; Lu, Q.; Wang, H.-T.; Xing, D.; Sun, J. Pressure stabilized lithium-aluminum compounds with both superconducting and superionic behaviors. *Phys. Rev. Lett.* **2022**, *129*, 246403.
- (11) Wang, Y.; Wang, J.; Hermann, A.; Liu, C.; Gao, H.; Tosatti, E.; Wang, H.-T.; Xing, D.; Sun, J. Electronically driven 1D cooperative diffusion in a simple cubic crystal. *Phys. Rev. X* **2021**, *11*, 011006.
- (12) Li, Y.-L.; Luo, W.; Zeng, Z.; Lin, H.-Q.; Mao, H.-k.; Ahuja, R. Pressure-induced superconductivity in CaC_2 . *P. Natl. Acad. Sci.* **2013**, *110*, 9289–9294.
- (13) Si, Q.; Yu, R.; Abrahams, E. High-temperature superconductivity in iron pnictides and chalcogenides. *Nat. Rev. Mater.* **2016**, *1*, 16017.
- (14) Zhang, L.; Wang, Y.; Lv, J.; Ma, Y. Materials discovery at high pressures. *Nat. Rev. Mater.* **2017**, *2*, 17005.
- (15) Drozdov, A.; Eremets, M.; Troyan, I.; Ksenofontov, V.; Shylin, S. I. Conventional superconductivity at 203 K at high pressures in the sulfur hydride system. *Nature* **2015**, *525*, 73–76.
- (16) Gor'kov, L. P.; Kresin, V. Z. Colloquium: High pressure and road to room temperature superconductivity. *Rev. Mod. Phys.* **2018**, *90*, 011001.
- (17) Chu, C. W. High-temperature superconductivity: Alive and kicking. *Nat. Phys.* **2009**, *5*, 787–789.
- (18) Zhang, D.; Chen, X.; Jiang, P.; Li, Y.; Zheng, X.; Liu, Z.; Miao, M.; Huang, H.-M.; Li, Y.-L. Pressure-tuned one- to quasi-two-dimensional structural phase transition and superconductivity in LiP_{15} . *Phys. Rev. B* **2022**, *105*, 094109.
- (19) Li, Y.-L.; Stavrou, E.; Zhu, Q.; Clarke, S. M.; Li, Y.; Huang, H.-M. Superconductivity in the van der Waals layered compound PS_2 . *Phys. Rev. B* **2019**, *99*, 220503.
- (20) Kim, D. Y.; Stefanoski, S.; Kurakevych, O. O.; Strobel, T. A. Synthesis of an open-framework allotrope of silicon. *Nat. Mater.* **2015**, *14*, 169–173.
- (21) Zhang, D.; Niu, H.; Li, Y.; Huang, H.-M.; Jiang, P.; Li, Y.-L. Tuning of electronic and optical properties of a predicted silicon allotrope: Hexagonal silicon h10-Si. *Phys. Rev. B* **2021**, *104*, 125201.
- (22) Solozhenko, V. L.; Andrault, D.; Fiquet, G.; Mezouar, M.; Rubie, D. C. Synthesis of superhard cubic BC_2N . *Appl. Phys. Lett.* **2001**, *78*, 1385–1387.
- (23) Solozhenko, V. L.; Kurakevych, O. O.; Andrault, D.; Le Godec, Y.; Mezouar, M. Ultimate metastable solubility of boron in diamond: Synthesis of superhard diamondlike BC_5 . *Phys. Rev. Lett.* **2009**, *102*, 015506.
- (24) Yang, X.; Yao, M.; Wu, X.; Liu, S.; Chen, S.; Yang, K.; Liu, R.; Cui, T.; Sundqvist, B.; Liu, B. Novel superhard sp^3 carbon allotrope from cold-compressed C_{70} peapods. *Phys. Rev. Lett.* **2017**, *118*, 245701.
- (25) Eremets, M. I.; Gavriliuk, A. G.; Trojan, I. A.; Dzivenko, D. A.; Boehler, R. Single-bonded cubic form of nitrogen. *Nat. Mater.* **2004**, *3*, 558–563.
- (26) Hirshberg, B.; Gerber, R. B.; Krylov, A. I. Calculations predict a stable molecular crystal of N8. *Nat. Chem.* **2014**, *6*, 52–56.
- (27) Ashcroft, N. Pressure for change in metals. *Nature* **2009**, *458*, 158–159.
- (28) Naumov, I. I.; Hemley, R. J. Origin of transitions between metallic and insulating states in simple metals. *Phys. Rev. Lett.* **2015**, *114*, 156403.
- (29) Shimizu, K.; Ishikawa, H.; Takao, D.; Yagi, T.; Amaya, K. Superconductivity in compressed lithium at 20 K. *Nature* **2002**, *419*, 597–599.
- (30) Deemyad, S.; Schilling, J. S. Superconducting phase diagram of Li metal in nearly hydrostatic pressures up to 67 GPa. *Phys. Rev. Lett.* **2003**, *91*, 167001.
- (31) Marqués, M.; McMahon, M. I.; Gregoryanz, E.; Hanfland, M.; Guillaume, C. L.; Pickard, C. J.; Ackland, G. J.; Nelmes, R. J. Crystal structures of dense lithium: A metal-semiconductor-metal transition. *Phys. Rev. Lett.* **2011**, *106*, 095502.
- (32) Schwarz, U.; Takemura, K.; Hanfland, M.; Syassen, K. Crystal structure of cesium-V. *Phys. Rev. Lett.* **1998**, *81*, 2711–2714.
- (33) McMahon, M. I.; Nelmes, R. J.; Rekhi, S. Complex crystal structure of cesium-III. *Phys. Rev. Lett.* **2001**, *87*, 255502.
- (34) Dong, X.; Oganov, A. R.; Cui, H.; Zhou, X.-F.; Wang, H.-T. Electronegativity and chemical hardness of elements under pressure. *P. Natl. Acad. Sci.* **2022**, *119*, e2117416119.
- (35) Zhang, X.; Zunger, A. Altered reactivity and the emergence of ionic metal ordered structures in Li-Cs at high pressures. *Phys. Rev. Lett.* **2010**, *104*, 245501.
- (36) Botana, J.; Miao, M.-S. Pressure-stabilized lithium caesides with caesium anions beyond the -1 state. *Nat. Commun.* **2014**, *5*, 4861.
- (37) Desgreniers, S.; Tse, J. S.; Matsuoka, T.; Ohishi, Y.; Tse, J. J. Mixing unmixables: Unexpected formation of Li-Cs alloys at low pressure. *Science Advances* **2015**, *1*, e1500669.

- (38) Oganov, A. R.; Glass, C. W. Crystal structure prediction using ab initio evolutionary techniques: Principles and applications. *J. Chem. Phys.* **2006**, *124*, 244704.
- (39) Oganov, A. R.; Lyakhov, A. O.; Valle, M. How evolutionary crystal structure prediction works—and why. *Acc. Chem. Res.* **2011**, *44*, 227–237.
- (40) Lyakhov, A. O.; Oganov, A. R.; Stokes, H. T.; Zhu, Q. New developments in evolutionary structure prediction algorithm USPEX. *Comput. Phys. Commun.* **2013**, *184*, 1172–1182.
- (41) Li, Y.-L.; Wang, S.-N.; Oganov, A. R.; Gou, H.; Smith, J. S.; Strobel, T. A. Investigation of exotic stable calcium carbides using theory and experiment. *Nat. Commun.* **2015**, *6*, 6974.
- (42) Hafner, J. Materials simulations using VASP—a quantum perspective to materials science. *Comput. Phys. Commun.* **2007**, *177*, 6–13.
- (43) Perdew, J. P.; Burke, K.; Ernzerhof, M. Generalized gradient approximation made simple. *Phys. Rev. Lett.* **1996**, *77*, 3865–3868.
- (44) Kresse, G.; Joubert, D. From ultrasoft pseudopotentials to the projector augmented-wave method. *Phys. Rev. B* **1999**, *59*, 1758–1775.
- (45) Henkelman, G.; Arnaldsson, A.; Jónsson, H. A fast and robust algorithm for Bader decomposition of charge density. *Comput. Mater. Sci.* **2006**, *36*, 354–360.
- (46) Giannozzi, P.; et al. QUANTUM ESPRESSO: a modular and open-source software project for quantum simulations of materials. *J. Phys.: Condens. Matter* **2009**, *21*, 395502.
- (47) Togo, A.; Tanaka, I. First principles phonon calculations in materials science. *Scr. Mater.* **2015**, *108*, 1–5.
- (48) Mizutani, U. Surface Properties and Engineering of Complex Intermetallics; World Scientific: 2010; pp 323–399.
- (49) Blatov, V. A.; Shevchenko, A. P.; Proserpio, D. M. Applied topological analysis of crystal structures with the program package ToposPro. *Cryst. Growth Des.* **2014**, *14*, 3576–3586.
- (50) Blatova, O. A.; Osipov, V. T.; Pavlova, V. E.; Solodovnikova, M. A.; Trofimychev, I. I.; Egorova, E. M.; Blatov, V. A. Local atomic configurations in intermetallic crystals: Beyond the first coordination shell. *Inorg. Chem.* **2023**, *62*, 6214–6223.
- (51) Blatov, V. A. Voronoi–Dirichlet polyhedra in crystal chemistry: theory and applications. *Crystallogr. Rev.* **2004**, *10*, 249–318.
- (52) O’Keeffe, M.; Peskov, M.; Ramsden, S.; Yaghi, O. The reticular chemistry structure resource (RCSR) database of, and symbols for, crystal nets. *Acc. Chem. Res.* **2008**, *41*, 1782–1789.
- (53) Aman, F.; Asiri, A. M.; Siddiqui, W. A.; Arshad, M. N.; Ashraf, A.; Zakharov, N. S.; Blatov, V. A. Multilevel topological description of molecular packings in 1,2-benzothiazines. *CrystEngComm* **2014**, *16*, 1963–1970.
- (54) Shevchenko, A. P.; Shabalin, A. A.; Karpukhin, I. Y.; Blatov, V. A. Topological representations of crystal structures: generation, analysis and implementation in the TopCryst system. *Science and Technology of Advanced Materials: Methods* **2022**, *2*, 250–265.
- (55) Grin, Y.; Savin, A.; Silvi, B. The Chemical Bond; Wiley: 2014; Chapter 10, pp 345–382.
- (56) Huang, T.; Liu, C.; Wang, J.; Pan, S.; Han, Y.; Pickard, C. J.; Helled, R.; Wang, H.-T.; Xing, D.; Sun, J. Metallic aluminum suboxides with ultrahigh electrical conductivity at high pressure. *Research* **2022**, *2022*, 9798758.
- (57) Allen, P. B.; Dynes, R. C. Transition temperature of strong-coupled superconductors reanalyzed. *Phys. Rev. B* **1975**, *12*, 905–922.
- (58) Li, Y.; Hao, J.; Liu, H.; Li, Y.; Ma, Y. The metallization and superconductivity of dense hydrogen sulfide. *J. Chem. Phys.* **2014**, *140*, 174712.
- (59) Duan, D.; Liu, Y.; Tian, F.; Li, D.; Huang, X.; Zhao, Z.; Yu, H.; Liu, B.; Tian, W.; Cui, T. Pressure-induced metallization of dense $(\text{H}_2\text{S})_2\text{H}_2$ with high- T_c superconductivity. *Sci. Rep.* **2014**, *4*, 6968.

□ Recommended by ACS

Interstitial Li^+ and Li^+ Migrations in the $\text{Li}_{2+x}\text{C}_{1-x}\text{B}_x\text{O}_3$ Solid Electrolyte

Xin-Yuan Feng, Fa Luo, et al.

OCTOBER 23, 2022
THE JOURNAL OF PHYSICAL CHEMISTRY C

READ ▶

Medium-Range Ordering in the Ionic Glass Electrolytes LiPON and LiSiPON

Andrew S. Westover, Nancy J. Dudney, et al.

MARCH 27, 2023
CHEMISTRY OF MATERIALS

READ ▶

Probing Capacity Trends in $\text{MLi}_2\text{Ti}_6\text{O}_{14}$ Lithium-Ion Battery Anodes Using Calorimetric Studies

K. Jayanthi, Alexandra Navrotsky, et al.

NOVEMBER 08, 2022
ACS OMEGA

READ ▶

Li-Ion Diffusion Correlations in LiAlGeO_4 : Quasielastic Neutron Scattering and Ab Initio Simulation

Sajan Kumar, Samrat L. Chaplot, et al.

OCTOBER 21, 2022
ACS APPLIED ENERGY MATERIALS

READ ▶

Get More Suggestions >